Are Nano-colloids Controlling Rare Earth Elements Mobility or Is It the Opposite? Insight from A4F-UV-QQQ-ICP-MS

Yasaman Tadayon, Lionel Dutruch, Delphine Vantelon, Julien Gigault, Aline Dia, Maxime Pattier, Mélanie Davranche

Are Nano-colloids Controlling Rare Earth Elements Mobility or Is It the Opposite? Insight from A4F-UV-QQQ-ICP-MS

Yasaman Tadayon, Lionel Dutruch, Delphine Vantelon, Julien Gigault, Aline Dia, Maxime Pattier, Mélanie Davranche

PII: S0045-6535(24)02061-7

DOI: https://doi.org/10.1016/j.chemosphere.2024.143164

Reference: CHEM 143164

To appear in: *ECSN*

Received Date: 30 April 2024

Revised Date: 1 August 2024

Accepted Date: 21 August 2024

Please cite this article as: Tadayon, Y., Dutruch, L., Vantelon, D., Gigault, J., Dia, A., Pattier, M., Davranche, M., Are Nano-colloids Controlling Rare Earth Elements Mobility or Is It the Opposite? Insight from A4F-UV-QQQ-ICP-MS, *Chemosphere*, https://doi.org/10.1016/j.chemosphere.2024.143164.

Are Nano-colloids Controlling Rare Earth Elements Mobility or Is It the Opposite? Insight from A4F-UV-QQQ-ICP-MS

Yasaman Tadayon [1], Lionel Dutruch[1], Delphine Vantelon[2], Julien Gigault[3], Aline Dia[1], Maxime Pattier[1] and Mélanie Davranche[1]*

1 Univ. Rennes, CNRS, Géosciences Rennes, UMR 6118, F-35000 Rennes, France.
2 Synchrotron SOLEIL, L'orme des merisiers, Saint Aubin BP48, 91192 Gif sur Yvette Cedex, France
3 TAKUVIK CNRS/ULaval, UMI3376, Université Laval, Quebec City, QC, Canada

*Corresponding author: Yasaman Tadayon
Email address: yasaman.tadayon@univ-rennes1.fr
Telephone number: +33620683696

HREE
MREE
LREE

ΣREE

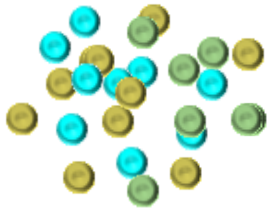

+

Fe/OM colloids

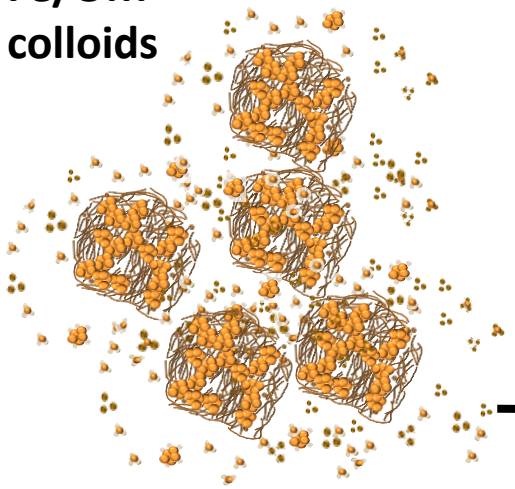

Bulk

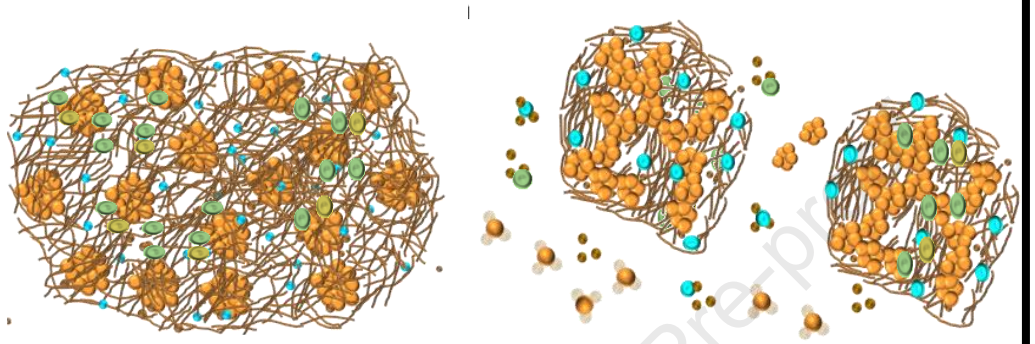

REE pattern shape < 3KDa

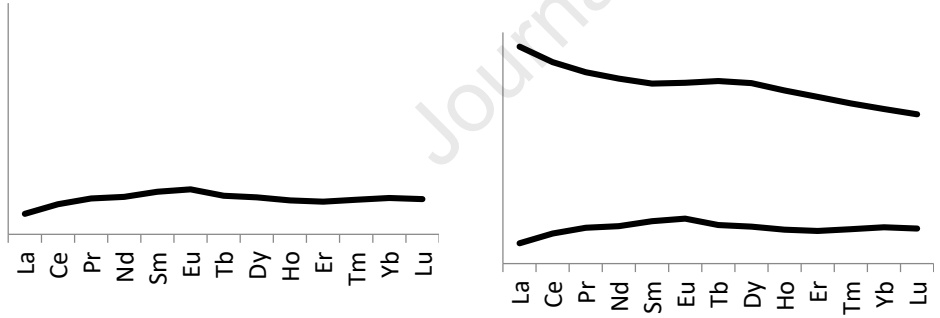

Nano colloids

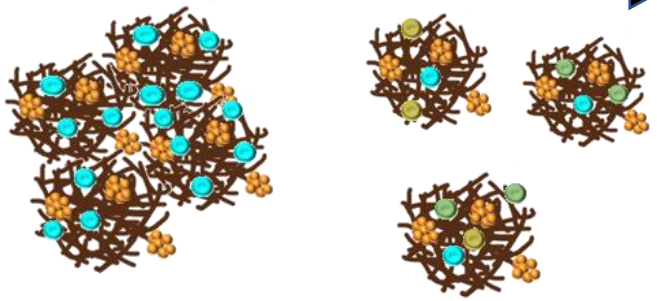

A4F-QQQ-ICP-MS

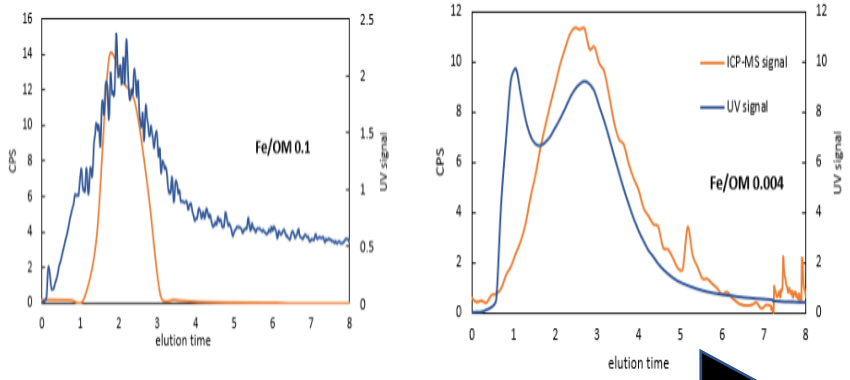

Ca ↘ REE ↘ pH ↗

Mobility ↗

Abstract

Rare earth element (REE) mobility in the environment is expected to be controlled by colloids. Recent research has detailed the structure of iron-organic colloids (Fe-OM colloids), which include both large colloids and smaller nano-colloids. To assess how these nano-colloids affect REE mobility, their interactions with REE and calcium (Ca) were investigated at pH 4 and 6. Using Asymmetric Flow Field Flow Fractionation (A4F) combined with UV and Triple Quadrupole Inductively Coupled Plasma Mass Spectrometry (QQQ-ICP-MS), Fe-OM nano-colloids were separated from bulk Fe-OM colloids and their REE and Ca content were analyzed. Without REE and Ca, nano-colloids had an average diameter of approximately 25 nm. Their structure is pH-dependent, with aggregation increasing as pH decreases. At high REE loadings (REE/Fe $\geq$ 0.05), REE induced a size increase of nano-colloids, regardless of pH. Heavy REE (HREE), with their high affinity for organic matter, formed strong complexes with Fe-OM colloids, resulting in large aggregates. In contrast, light REE (LREE), which bind less strongly to organic molecules, were associated with the smallest nano-colloids. Low REE loading did not cause noticeable fractionation. Calcium further enhanced the aggregation process at both pH levels by neutralizing the charges on nano-colloids. These findings indicate that REE can act as aggregating agent controlling their own mobility, and regulating colloid transfer.

Key words: Iron organic nano-colloids, Rare Earth Elements (REE), Environmental Factors, Asymmetric Flow Field Flow Fractionation (A4F) Technique, Size Fractionation

1 Introduction

Colloids are known to be a major controlling factor in the mobility of numerous chemical elements and notably metals (i.e. Lead et al., 1997; Pokrovsky & Schott, 2002; Town et al., 2012). They are naturally formed by microbial activity, mineral weathering, soil erosion and permafrost thawing (Lead et al., 2006). They can also originate from in-situ precipitation of supersaturated solutions in response to redox alternations as in wetlands (Ryan & Elimelech, 1996). They can be mono- (ex. clay minerals and Al and Fe oxyhydroxide) or multiphasic/composite (ex. Fe-organic matter (OM) colloids). The release of colloids into the environment increases with global climate change, particularly those comprised of minerals and organic matter (OM), in response to various factors such as soil erosion, flooding due to intensified precipitation, heightened microbial activity due to increased temperatures, mineral weathering, and permafrost thawing due to rising temperatures.

Among colloids, due to metals high affinity for Fe phases and natural OM, Fe-OM colloids are considered as a major transport mechanism for metals in soils and freshwaters (O. S. Pokrovsky et al., 2010; O. S. Pokrovsky & Schott, 2002; Vasyukova et al., 2010). Colloids are indeed considered as nano vectors for trace metal due to their high specific surface (Hassellöv & von der Kammer, 2008). For heterogeneous Fe-OM colloids, scientific community generally considered that Fe occurs as nano oxides embedded in colloidal OM, which controls their size. However, Guénet et al., (2017) demonstrated that several phases are present. Iron has a fractal organization in which Fe nano beads aggregate to form primary aggregates, which then aggregate to form secondary aggregates. The OM is present as molecules adsorbed on primary aggregates and large colloids that surround the secondary Fe aggregates. The particles sizes are ranging from 0.8 nm for the Fe nano beads to 700 nm for the OM colloid. Beauvois et al., (2020, 2023) demonstrated

that this structural organization is dynamic, i.e. evolving in the presence of major cations such as Ca and Al. In aquatic systems, Ca is a major ion, typically present at concentrations ranging from 10^{-2} to 10^{-4} mol L^{-1} (Christl, 2012). Calcium forms cationic bridges between the organic macromolecules of the OM colloids, in response to its strong affinity for OM carboxylic groups (Kalinichev & Kirkpatrick, 2007; Ouatmane et al., 1999). No interaction occurs between Ca and Fe phases. The Ca bridges result in an opening of the OM colloid structure and the aggregation of soluble organic molecules leading to a non-colloidal, micrometric Ca-branched OM network, where Fe aggregates are embedded (Beauvois et al., 2020).

Rare earth elements (REE) are a group of chemically similar elements. They are naturally present in trace amounts in soil solution and groundwater. However, their increased use has led to higher concentrations in the environment. They enter the environment through multiple pathways, including landfill disposal of consumer and industrial products, emissions from mining processing, and effluents from industrial processes. Soils in mining areas have REE concentrations at least 100 times higher than natural background levels. Reported concentrations of REE in soils range from 30.86 to 327.50 mg kg^{-1}, in surface waters from 0.17 to 160.06 µg L^{-1}, and in sediments from 0.0002 to 9850 mg kg^{-} (Ferreira et al., 2021; X. Li et al., 2013; Loell et al., 2011; Ma et al., 2019; Strakhovenko et al., 2023; Tang et al., 2020). Additionally, agricultural soils are increasingly contaminated with REE due to phosphate-based fertilizers. These elements are progressively infiltrating ground and surface waters, posing environmental risks. Evaluating these risks requires deciphering their mobility pathways, with speciation and physicochemical conditions like pH and ligands being key factors. The mobility of REE are controlled by various factors such as aqueous complexes (both organic and inorganic) and sorption onto organic and inorganic colloids and particles (Goyne et al., 2010; Laveuf & Cornu, 2009; Pourret et al., 2007a; Sonke & Salters, 2006a;

Gwenzi et al., 2018; Klaine et al., 2008). Rare earth elements have high affinity for Fe phases and natural OM (Bau, 1999; Liu et al., 2017; Marsac et al., 2010; Pourret et al., 2007b; Quinn et al., 2006; Schijf & Marshall, 2011; Sonke, 2006; Sonke & Salters, 2006b) and therefore for Fe-OM colloids. Onto OM colloid, at high REE loading, REE are mainly bound to carboxylic sites as bidentate complexes, middle REE (MREE) being more complexed than light (LREE) and heavy (HREE) REE. By contrast, at low REE loading, REE form strong chelate complexes, HREE are then more adsorbed than LREE and MREE (Marsac et al., 2011). Onto Fe oxyhydroxides, REE are bound to OH sites as weak and strong complexes, HREE having more affinity for the surface than LREE and MREE (Liu et al., 2017). Onto Fe-OM colloids, Tadayon et al. (2023) demonstrated that REE binding is dominated by their complexation to OM phases (macromolecule and colloids), no adsorption occurring on the Fe phases. However, in their experiments, these authors only considered the bulk colloids, namely all Fe and OM phases.

By contrast to the understanding of colloid speciation and size fractionation in surface water, our knowledge of the distribution and mobility of REE regarding the small aggregates (Fe primary aggregates and bound organic molecules) of the Fe-OM colloids through soil solution and freshwater has remained considerably limited. However, Li et al. (F. Li et al., 2021) showed that the smallest colloids (0.6-25 nm), so called nano-colloids, move at a greater velocity than solutes due to their size and charge exclusion effects, therefore by-passing the less mobile water domains in microscopic pores and restricted transport channels (Afsar et al., 2023). Understanding the behavior of the smallest colloidal phase within these heterogeneous Fe-OM colloids is thus critical for determining the real mobility and environmental fate of REE in natural environments.

Several techniques were employed for the analysis and characterization of colloids, including Transmission Electron Microscopy (TEM), Dynamic Light Scattering (DLS), and Fourier-Transform Infrared Spectroscopy (FTIR) (Buffle & Leppard, 1995; Halter et al., 2010; Nuttall & Kale, 1993; Philippe & Schaumann, 2014; K. A. Roberts et al., 2004; Walther, 2003). While these techniques provide valuable information on size, morphology, and functional groups, they often lack the ability to separate and characterize the colloids. By contrast, Asymmetric Flow Field Flow Fractionation (A4F) is a versatile technique that enables the separation and characterization of colloidal particles based on their size and charge (Gigault et al., 2017). The A4F technique is based on diffusional properties of particles within a parabolic flow profile, achieved by the application of a cross-flow field (Gigault et al., 2014; Schimpf et al., 2000). The inorganic element content of various colloid size fractions can be determined using the A4F and inductively coupled plasma mass spectrometer (ICP-MS) in combination (Prestel et al., 2005). This technique is widely used for the size-based characterization of colloidal suspensions which combines the principles of cross-flow, gravitational sedimentation, and an applied electric field to separate particles based on their hydrodynamic size. The technique was successfully applied to various colloidal systems, allowing for the determination of size distributions, molar mass distributions, and surface properties of colloids (Giddings, 1993; Müller et al., 2015; Runyon et al., 2014; Saito et al., 2013; Wagner et al., 2014).

The present study therefore aims at investigating the REE binding onto the smallest and most mobile phases constitutive of Fe-OM colloids, so-called Fe-OM nano-colloids. This nano-colloids behavior (size and aggregation) was compared before and after REE adsorption at pH 4 and 6 and with and without Ca as coagulating agent by using the A4F technique. Earlier investigations employing sequential ultrafiltration and dialysis techniques have revealed the distribution of

colloidal trace elements among small (1–10 kDa) organic and larger (10 kDa–450 nm) iron-rich colloids. This distribution pattern appears to be intricately linked to the chemical properties of the elements, as documented in several studies (Dahlqvist et al., 2007; O. Pokrovsky et al., 2006; O. S. Pokrovsky & Schott, 2002). The present study focuses specifically on nano-colloids with hydrodynamic diameter (D_H) between 20 kDa and 400 nm. The selection of this size range is essential driven by the A4F technique and for a comprehensive investigation of the mobility and transport dynamics innate to these nano-colloids.

The findings of this study make a significant contribution to advancing our fundamental comprehension of the behavior exhibited by nanometric constituents within heterogeneous Fe-OM colloids, as well as the role of REE as potential aggregating agent. Furthermore, this study sheds light on the influence of various parameters, including REE concentration, pH levels, and the addition of Ca to the structure of colloids.

2 Materials and Methods

2.1 Fe-OM colloids synthesis

The colloids were synthesized using Leonardite humic acid (HA) obtained from the International Humic Substances Society. The synthesis process involved the preparation of aqueous solutions with ultra-pure water from a Milli-Q-Integral system (Millipore). The colloidal samples were denoted as (Fexx-OMyy) and (Caxx-Feyy) for those containing Ca, whereas xx and yy correspond to the Fe/OM ratios and to the Ca/Fe, respectively.

The synthesis of Fe-OM colloids was achieved through a titration method using Fe(II) and Ca(II) solutions, following the detailed protocol provided by Guénet et al., (2016) and Beauvois

et al., (2020, 2021). The titration solution was prepared by dissolving $FeCl_4.4H_2O$ (Sigma Aldrich) at a concentration of 1000 mg L^{-1} Fe(II) and $CaCl_2.2H_2O$ (Sigma Aldrich) at a concentration of 1000 mg L^{-1} Ca(II). The ionic strength (IS) of both the titration and HA solutions was maintained at 5 mM using NaCl.

The titration solution was added to a suspension of HA at a concentration of 700 mg L^{-1} to synthesize colloids at ratio 0.25 Fe to OM (mol/mol), and 0.5 Ca to Fe (mol/mol) for the colloids containing Ca, at a constant flow rate of 0.05 mL min^{-1} using an automated titrator (Titrino 794, Metrohm). The pH of the system was maintained at 6.5 by the addition of 0.1 M NaOH using a pH measurement accuracy of ±0.04 pH unit (Titrino 794, Metrohm). The selected ratios and pH were aligned with those documented for natural wetlands by Dia et al., (2000) and Pourret et al., (2010).

2.2 REE Adsorption Experiments

A series of batch adsorption experiments were conducted to investigate the adsorption behavior of REEs onto Fe-OM colloids. Under controlled conditions, different initial concentrations of REE were added to the colloids to get adsorption isotherms. Colloid size was examined after a 100-times dilution at the same ionic strength without modifying the Fe/OM ratios. The dilution did not modify the colloids size and stability significantly as shown by DLS measurement (Tadayon et al., 2024). The detailed parameters are presented in the Supplementary Information materials (SI 1.1). The REE stock solution (CCS-1, Inorganic Venture) containing lanthanides from La to Lu was used. The REE/Fe ratios of 0.1, 0.01, 0.05, 0.004, and 0.0008 (mol/mol) were selected based on samples obtained from mining areas in Portugal (Forsyth et al., 2023). The adsorption of REE onto

colloids was investigated using a batch equilibrium method. After the addition of REE to the colloidal suspension, the pH was adjusted to 4 and 6 using HNO_3 and/or NaOH solutions (0.1 to 1 mol L^{-1}). These pH values were deliberately chosen to facilitate the observation of distinct REE patterns corresponding to varying REE loading levels, reflecting the quantity of adsorbed REE. The equilibrium time was set to 48 hours based on previous studies (Catrouillet et al., 2019). Upon reaching equilibrium, the suspensions underwent a subsequent step involving ultrafiltration using Polyether Sulfone (PES) membranes with a molecular weight cutoff of 3 kDa (Sartorius). This procedure was conducted within ultrafiltration cells, serving the purpose of effectively separate the adsorbed REE from the solution. To ensure the highest standards of purity and precision in the separation process, the ultrafiltration cells were subjected to rigorous cleaning procedures. Initially, they were cleaned with a solution of 0.05M HNO_3 and subsequently subjected to three sequential rinses with ultra-pure water. This stringent protocol was enacted to reduce the total dissolved organic carbon concentration to a level below 0.2 mg L^{-1}. Following the ultrafiltration process, all samples underwent an additional step of acidification, involving treatment with a 0.37 mol L^{-1} HNO_3 solution, in preparation for measurements employing Inductively Coupled Plasma Mass Spectrometry equipped with triple quadrupole (QQQ-ICP-MS).

2.3 REE quantification

The concentrations of REE were quantified utilizing a QQQ-ICP-MS instrument (Agilent Technologies-8900), equipped with two quadrupole mass filters, providing enhanced sensitivity and reduced backgrounds compared to single quadrupole ICP-MS. This configuration is particularly advantageous for the analysis of particulate pollutants. Calibration curves were established and validated using certified reference materials (SLRS-6, National Research Council).

An internal standard, rhodium solution, was employed to correct for instrumental drift and potential matrix effects. The average limit of quantification for REE was determined by measuring 10 blank samples. Following the calculation of the standard deviation (SD), the limit of quantification (LOQ) was computed using the following formula (LOQ = 10×SD) and it was established at 0.1 ppt. Given that the upper limit of the REE calibration curve was 5 ppb, sample dilution was performed to ensure this value was not exceeded.

2.4 Nano-colloids fractionation and characterization: A4F-UV analysis

The characterization of the colloids was performed using A4F coupled to UV (AF4-UV) (Wyatt Technology). The channel thickness was fixed using a 250-µm Mylar film, and the channel dimensions were 26.5 cm in length and narrowed from 2.1 to 0.6 cm in width. The accumulation wall was defined by a 20 kDa molecular mass cutoff Polyether sulfone (PES) membrane (Wyatt Technology). The method was previously described by (Gigault et al., 2017). A total of 300 µL of each sample was injected into the A4F instrument. The A4F instrument was calibrated using polystyrene spherical models (PSL, NIST traceable standard) to correlate the elution time with the equivalent hydrodynamic diameter (D_H). The detailed parameters are presented in the Supplementary Information materials (SI 1.2).

2.5 REE size fraction characterization: A4F- QQQ-ICP-MS

A coupled QQQ-ICP-MS (Agilent Technologies 8900) was established at the A4F outlet, enabling the determination of elemental composition in relation to nano-colloids fraction. The operating settings for AF4-QQQ-ICP-MS analysis were selected in order to simultaneously monitor REE bound to the nano-colloids fractions. The flow rate of A4F at 0.5 mL min^{-1}

underwent a split through a T-piece. Before reaching the QQQ-ICP-MS via the peristaltic pump, the final solution was adjusted to 0.4 mL min^{-1} and then directed to the nebulizer of the spectrometer. The acquisition time for each element in O_2 mode was set to 1 second.

3 Results and discussion

3.1 Nano-Colloids in Sub-3kDa Fraction

Tadayon et al., (2024) provided evidence of REE binding to small organic molecules in fractions below 3 kDa, as indicated by the observed REE pattern shape at lower REE loadings. Prior to conducting experiments, it was imperative to confirm the presence of Fe-OM nano-colloids rather than solely small organic molecules within this fraction. Thus, QQQ-ICP-MS were coupled with the A4F-UV to analyze Fe at low REE concentrations (REE/Fe 0.004). The intensity of the Fe signal was expressed as counts per second (CPS). The fractograms representing the UV signal (amount of nano-colloids) and the Fe amount (CPS) according to the elution time (evolution of the nano-colloids size) were plotted in Figure 1 for Fe/OM = 0.25 and REE/Fe = 0.004. Analysis of the UV signal reveals the presence of two distinct size populations. The first at 1 min corresponding to nano-colloids with hydrodynamic diameters (D_H) ranging from 20 kDa to 3 nm according to the size calibration curve (SI. Figure S1), with small or insignificant amount of Fe and a second at 3.5 min corresponding to nano-colloids of 25 nm which is synchronized with a Fe peak. These results support the hypothesis of Tadayon et al. (2024) proposing the presence of small organic nano-colloids and provide evidence of the presence of Fe-OM nano colloids.

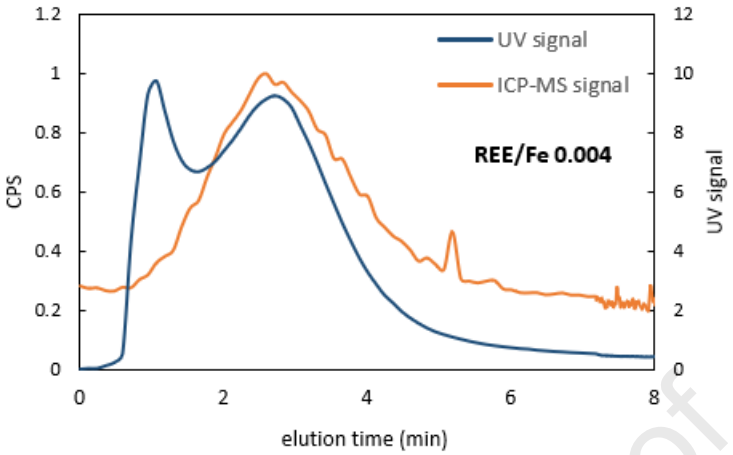

Figure 1. Overlaid fractograms of UV signal for nano-colloids and QQQ-ICP-MS signal of Fe at pH 6 for REE/Fe 0.004

3.2 pH and REE adsorption impact on nano-colloids size

The fractograms representing the UV signal (amount of nano-colloids) according to the elution time (evolution of the nano-colloids size) were plotted for Fe/OM = 0.25 and the different REE/Fe ratios (i.e. 0.1, 0.05, 0.0129, 0.004, 0.0008) at pH 4 and pH 6 in Figures 2A and 2B, respectively. The REE distribution coefficients (log K_d) patterns of the bulk colloids were plotted at pH 4 and pH 6 in Figures 2C and 2D, respectively for Fe/OM = 0.25 and different REE/Fe ratios (0.1, 0.05, 0.0129, 0.004, 0.0008).

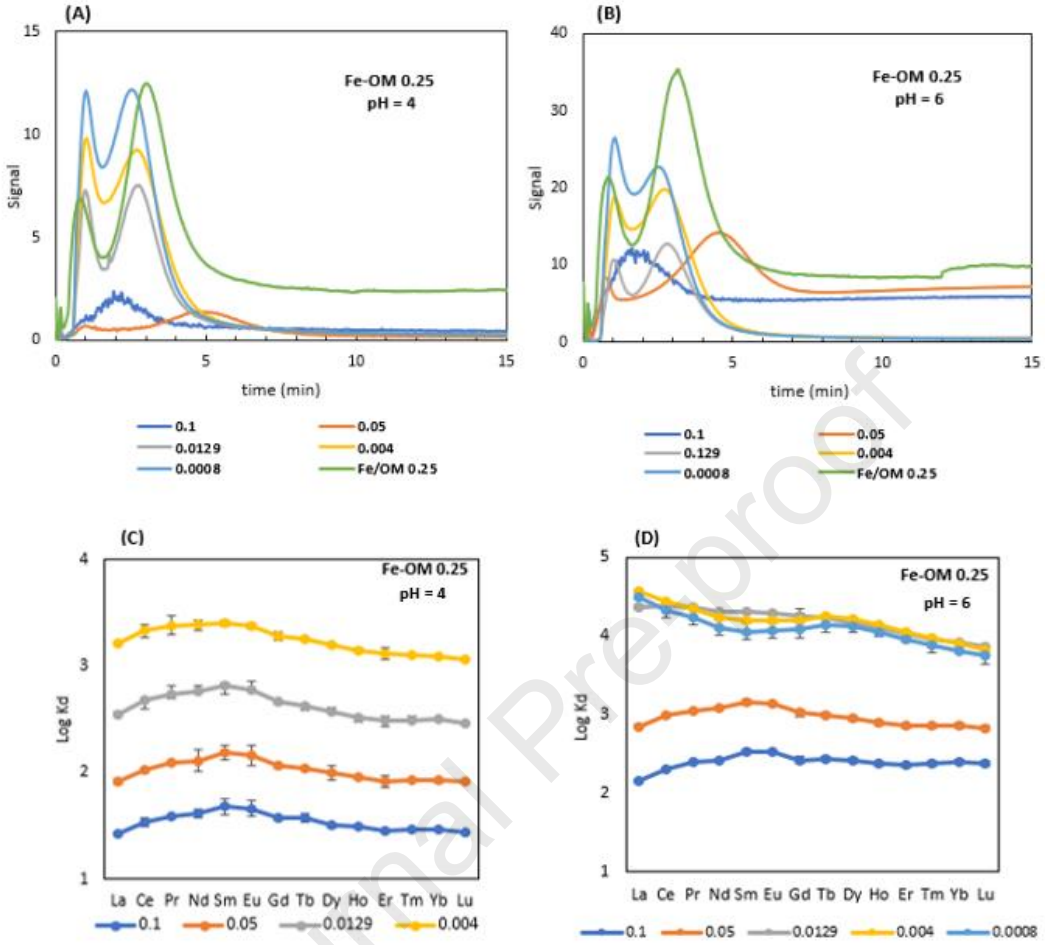

Figure 2. Fractograms (UV trace at 254 nm) of colloids (Fe-OM=0.25) without and with REE extracts at pH 4 (A) and 6 (B). Variation of Log K_dREE patterns in the bulk colloids relative to the REE/Fe ratios (0.1, 0.05, 0.0129, 0.004, 0.0008), at pH 4 (A) and pH 6 (C). For all samples, Fe/OM = 0.25.

For the reference colloids (i.e. without REE), the fractogram exhibits a first peak at 1 min corresponding to particles with hydrodynamic diameters (D_H) ranging from 20 kDa to 3 nm according to the size calibration curve (SI. Figure S1) at both pH (Figures 2A and 2B). These fractions were typically non-colloidal in nature and corresponded to low-molecular-weight OM (Chevalier et al., 2018). A second peak at 3.5 min refers to ~ 25 nm- (average due to size

polydispersity around this value) nano-colloids (D_H), confirming that the larger colloids, namely the secondary Fe aggregates surrounded by the OM colloid with geometric diameter (D_g) of ~ 700 nm, did not pass through the A4F channel. This peak may represent primary aggregates, which were previously reported to have a geometry diameter (D_g) of approximately 6 nm as measured by transition electron microscopy (TEM, dry sample) (Beauvois et al., 2020; Guénet et al., 2016). However, due to the typical phenomenon where D_H exceeds D_g (G. C. Roberts, 1975; Skliar & Chernyshev, 2019), their average D_H was measured at ~25 nm. This discrepancy in size is attributed to the existence of a low-mass or low-density shell enveloping these particles, contributing to an increase in their hydrodynamic dimensions. At pH 6, the UV signals showed more intense absorbance (3 times) than at pH 4. This results indicated an aggregation of the nano-colloids at acidic pH due to organic macromolecules aggregation (Pédrot et al., 2010).

At both pH for REE/Fe $\geq$ 0.05, a transition from the normal mode to the steric mode was obvious in UV signals. This transition was characterized by noticeable shifts in elution times, broader peaks, and deviation from the idealized behavior typically observed in the normal mode. In the "steric mode elution," there was a reversal in the size-elution time relationship, meaning that larger species eluted first. This shift from the normal mode to the steric mode of elution typically occurs when particle sizes reach the micrometer range (Beckett & Giddings, 1997). The concentration of REE exerted thus a significant impact on the elution behavior of nano-colloids. This influence included an increase in particle size and the promotion of the aggregation, regardless of the prevailing pH conditions. This process indicated the analysis of relatively large particles, whose size became comparable to or exceeded the pore size of the stationary phase, resulting in modified elution behavior in reverse (Dai et al., 2021; Phelan & Bauer, 2009).

At pH 4, for REE/Fe ≤0.0129, a subtle shift of the peaks to the left (3.5 against 2.5 min) was observed as compared to the reference colloid. This shift indicated that these particles have undergone a change in their elution behavior, typically associated with a size decrease or an alteration of the structure. Furthermore, as the REE/Fe ratios decreased, the nano-colloids UV signal increased, indicating that their concentration increased. With the increasing content of REE, both peaks intensity slightly decreased, indicating a decrease in the larger nano-colloids concentration and a concurrent increase in the smallest colloids, demonstrating the influence of REE on the nano-colloid size.

From pH 4 to pH 6, several changes were observed, although one can still observe the same trend of shift in the peak position and intensity with the REE content, demonstrating the same influence of REE on the nano-colloid size. However, from pH 4 to pH 6, the intensity of the peaks at 1 and 2.5 min slightly decreased for a given REE content (Figure 2B), indicating a decrease in the larger nano-colloids concentration and a concurrent increase in the smallest colloids with increasing pH. Additionally, a gradual narrowing of the peak width occurred with the pH increase, indicative of a more uniform size distribution at pH 6. Consequently, the transition from pH 4 to pH 6 involved the disaggregation of large-sized colloids to smaller-sized colloids, ultimately leading to a more uniform size distribution (Xu et al., 2018). These findings are also in accordance with the results reported by Yang et al. (Yang et al., 2010), who noted an enhanced UV_{254} decrease with the pH decrease.

Beyond the influence of pH, it is important to note that REE themselves have an impact on nano-colloid size. At pH 4, A MREE downward concavity associated to the REE binding to OM (Davranche et al., 2005; Marsac et al., 2010, 2013; Tadayon et al., 2024) was observed but no

significant variations of the pattern occurred with the REE/Fe ratio (Figure 2C). The protonation of binding sites restricted the adsorption of REE and the formation of multidentate complexes or strong complexes with HREE. Consequently, at pH 4 the adsorption of REE was limited to weak complexes preventing the REE pattern variation with the REE/Fe ratio (loading effect). As a result, the leftward shift of the second peak of the A4F-UV signals at pH 4 remained limited for all REE concentrations (Figure 2A).

At pH 6, the REE log K_d for the bulk colloids were notably higher than at pH 4, indicating a higher quantity of bound REE (Figures 2C and 2D). For REE/Fe $\geq$ 0.05, the REE patterns exhibited the same characteristic MREE downward concavity than at pH 4 for all the REE contents. However, for REE/Fe $\leq$ 0.0129, the patterns displayed an uncommon enrichment of LREE and a depletion of HREE (Figure 2D). Tadayon et al., (2024) demonstrated that at pH 6, in the fraction <3 kDa, REE were complexed to small organic molecules at condition of low loading which resulted in REE pattern exhibiting a preferential complexation of HREE. Due to the fractionation at 3 kDa of these small organic molecules from the bulk colloids, the inverse REE pattern was imposed to the fraction > 3kDa. This uncommon pattern was therefore an artifact of the ultrafiltration that however demonstrated that at pH 6, small organic molecules are solubilized from the bulk colloids and that they have strong affinity for REE. On the A4F-UV signals, these small organic molecules released from nano-colloids corresponded to the leftward shift and the decrease of the UV intensity of the peak at 3 min (nano-colloids) (Figure 2B).

3.3 **Effect of Ca**

The same experiments were performed with Ca (Figure 3). At both pH, 4 and 6, as compared to the reference colloids the addition of Ca at Ca/Fe = 0.5 resulted in a decrease of the UV signal as compared to the reference colloids and thus, of the nano-colloids amount in response to their aggregation. However, the impact of Ca was different at pH 4 and pH 6.

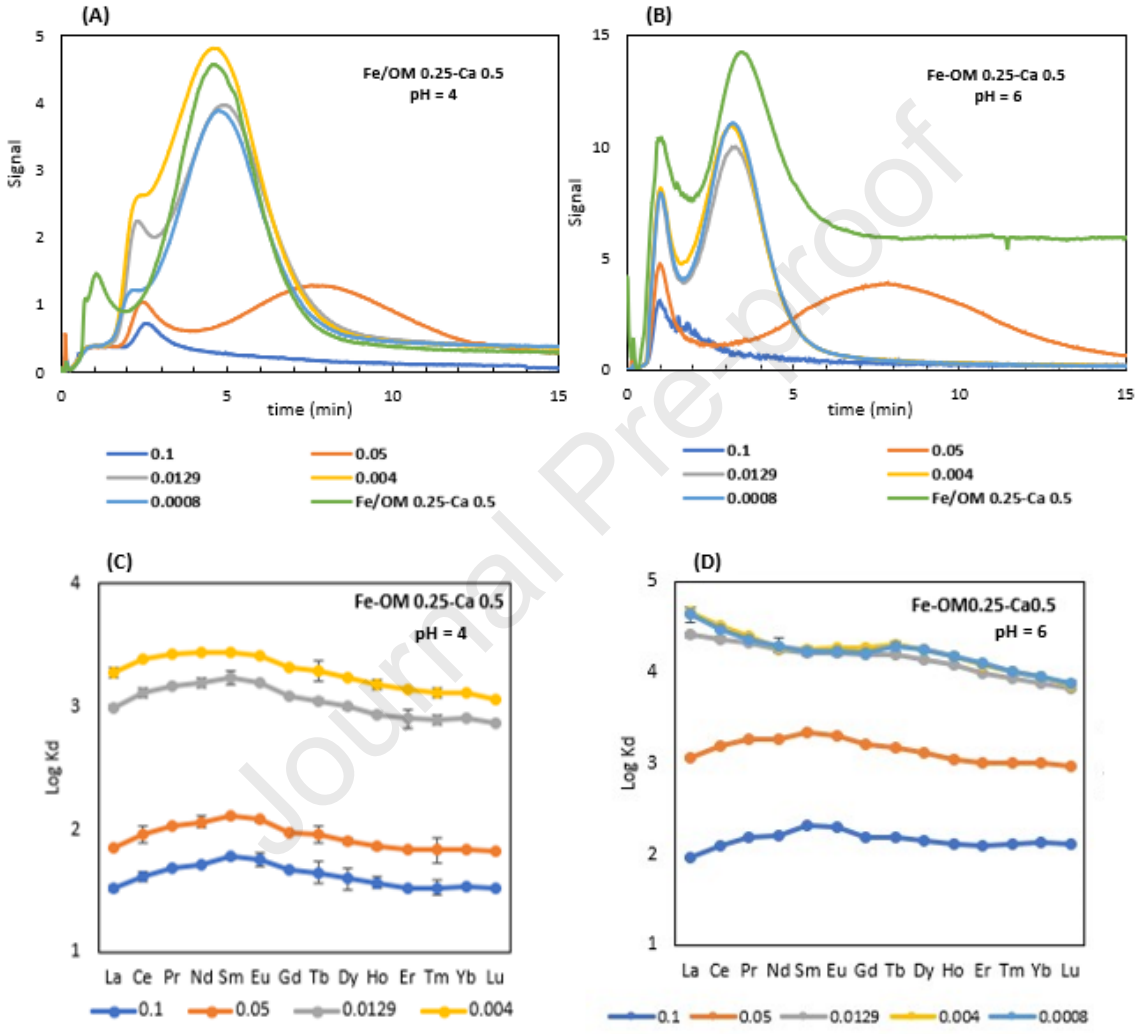

Figure 3. Fractograms (UV trace at 254 nm) of colloids with Ca, without and with REE extracts at pH 4 (A) and 6 (B). Variation of Log K_d REE patterns relative to the REE/Fe ratios (0.1, 0.05, 0.0129, 0.004, 0.0008) at Fe/OM 0.25 and Ca/Fe 0.5, at pH 4 (A) and pH 6 (C)

At pH 4, in presence of REE, the addition of Ca involved a noticeable rightward shift of the first peak as compared to the reference colloids (without REE) from 1 to 2 min whereas the first peak remained at 1 min for the sample without REE. Simultaneously, the second peak shifted from 3.5 to 4.5 min. This shift was accompanied by a significant decrease in the UV signal intensity as compared to the colloids without Ca under the same conditions (Figure 3A). Both indicated an increase of the size and a decrease amount of nano-colloid with Ca. This transformation became evident through the appearance of a distinct, sharp peak at 4.5 min. Peaks at 3.5 and 4.5 min indicated that aggregates measured ~18 nm and ~45 nm (D_H) against ~18 nm and ~25 nm for the reference. At pH 4, the protonation of nano-colloid binding sites limited the Ca complexation. Figure 4 illustrates Ca concentration into the solution as a function of REE concentration in presence of Ca at pH 4. The Ca concentration in the solution was therefore higher at pH 4 (92-113.91 µg L^{-1}) than at pH 6 (0.05- 0.4 µg L^{-1}) whichever REE/Fe ratios were considered (Figure 4). The resulting charge neutralization promoted intramolecular contraction or intermolecular aggregation of OM colloids (Au et al., 1999; Kloster et al., 2013). At pH 6, a higher amount of Ca was complexed with colloids, leading to the formation of cationic bridges between colloids. However, the UV signal intensity decreased, indicating a decrease in the particle amount (Figure 2B). A small rightward shift of the UV peak from 3.5 (reference colloids) to 3.1 min also occurred indicating a small decrease in the nano-colloids size. Both results combined with the REE pattern of the bulk colloids (Figures 3B and 3D) can be explained by the release of very tiny nano-colloids from the largest nano-colloids in the fraction < 20 kDa (outside of the channel). These results showed also that pH decrease is more efficient than Ca to aggregate Fe-OM colloids with and without REE. By contrast, when REE/Fe ratio exceeded 0.0129, a steric effect occurred at both pH indicating a strong aggregation of the colloids and the formation of a micrometric network.

While the REE log K_d patterns did not undergo significant changes as without Ca, the log K_d values indicated an increase of the REE adsorption at both pH in response to the increasing adsorption capacity due to the expansion of the colloid structure (Beauvois et al., 2021). At pH 4, a significant proportion of the binding sites is protonated, limiting Ca and REE adsorption. At pH 6, for the lowest REE/Fe ratio and with Ca, the peak at 3.5 min (reference) shifted to 3 min suggesting that the REE occurrence decreased the nano-colloids size (Figure 3B).

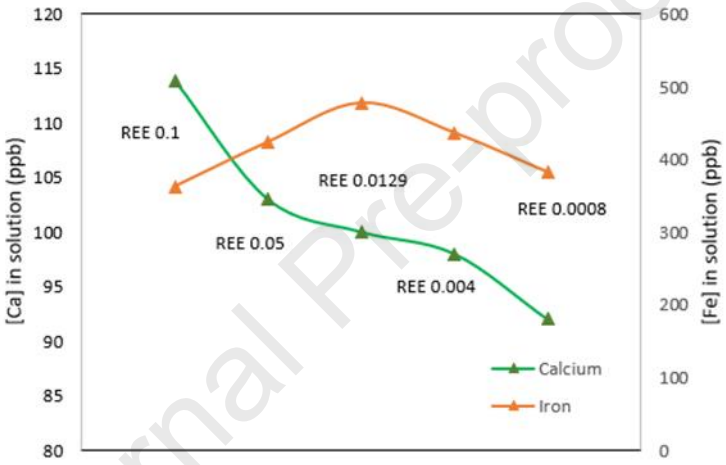

Figure 4. Ca concentration into the solution as a function of REE concentration in presence of Ca at pH 4

Therefore, interactions between REE and nano-Fe-OM colloids (D_H <400 nm) led to an increase of the nano-colloid size, as demonstrated by A4F-UV analysis. Rare earth elements seem to act as an aggregating agent as suggested in previous studies (Elderfield et al., 1990; Merschel et al., 2017). The nano-colloid size increase was higher at pH 4. This process is associated with OM aggregation/disaggregation within the bulk Fe-OM colloids (Baalousha, 2009; Baalousha et al., 2008; Philippe & Schaumann, 2014; H. Xu et al., 2018). At pH 6, with and without Ca, tiny

OM colloids (sized < 20 kDa) were released. Rare earth elements form with this tiny OM nano-colloids strong multidentate complexes as demonstrated by the REE log Kd patterns.

3.4 REE distribution in nano-colloids fractions

To demonstrate the presence of Fe-OM nano-colloids and the effective binding of REE to nano-colloids, A4F-UV were combined with QQQ-ICP-MS to obtain information regarding their distribution with their size fractions. The intensity of the Fe and REE signal was expressed as counts per second (CPS) and each CPS was normalized by the total signal of each REE and total Fe. Ratio of REE/Fe 0.1 at pH 6 were selected to observe steric effects, and REE/Fe0.004 at pH 6 were selected for low concentration of REE. Figures 5A and 5B shows the A4F-UV-QQQ-ICP-MS fractograms of REE at both ratios.

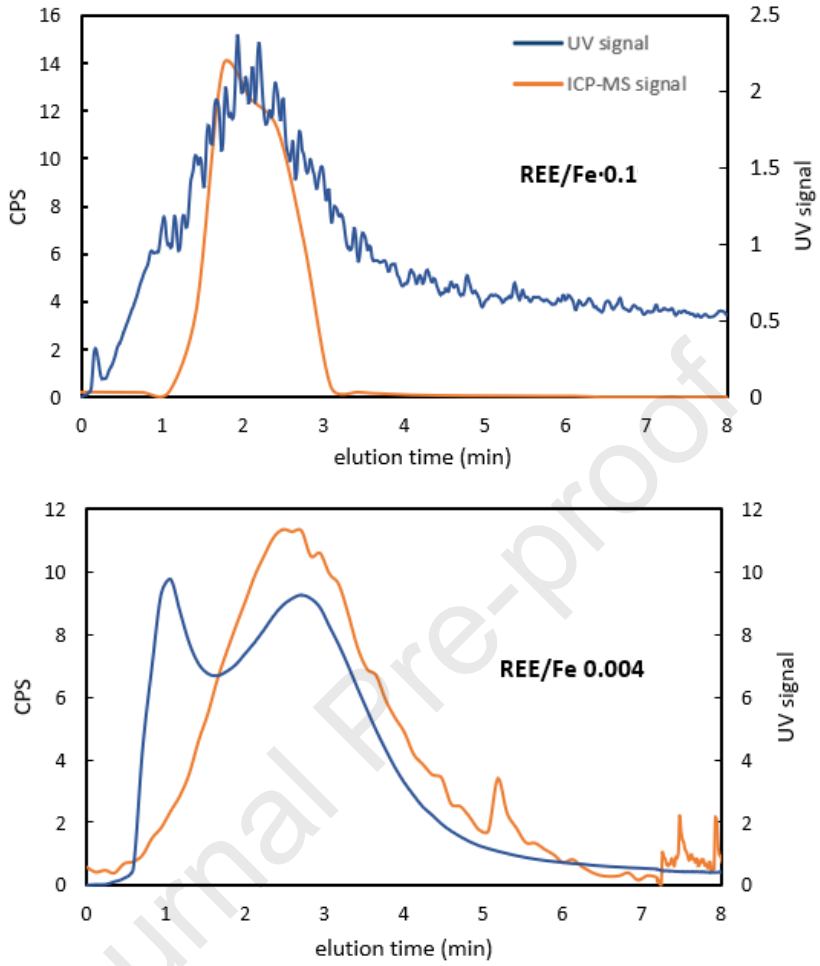

Figure 5. Overlaid fractograms of UV signal for nano-colloids and QQQ-ICP-MS signal of ΣREE at different fractionations at pH 6 A) for REE/Fe 0.1 and B) for REE/Fe 0.004. The REE signal corresponds to the sum of each REE signal.

The UV and QQQ-ICP-MS signals showed a conspicuous alignment indicative of the binding of REE to nano-colloids both at low and high REE/Fe ratios. For REE/Fe ratio 0.004, UV signal exhibited two peaks at 1 min (~18 nm) and 2.8 min (~24 nm) indicating the presence of 2 nano-colloids size (Figure 5). The QQQ-ICP-MS signal of REE exhibited, however, only one peak at 2.8 min (~24 nm) demonstrating that at pH 6, REE were mainly bound to the largest size fraction

of the Fe-OM nano-colloids. Moreover, the REE QQQ-ICP-MS signal exhibited only one peak at 2.8 min, indicating that no or few fractionations occurred between REE at the surface of the largest fraction of the Fe-OM nano-colloids. By contrast at REE/Fe ratio 0.1, a singular UV peak, attributed to steric elution mode showed that small Fe-OM nano-colloids were eluted before large Fe-OM nano-colloids and that a micrometric network was formed. A dual QQQ-ICP-MS peak with peaks maximum at 1.5 and 2.3 min denoted a fractionation between REE in different size fractions of Fe-OM nano-colloids.

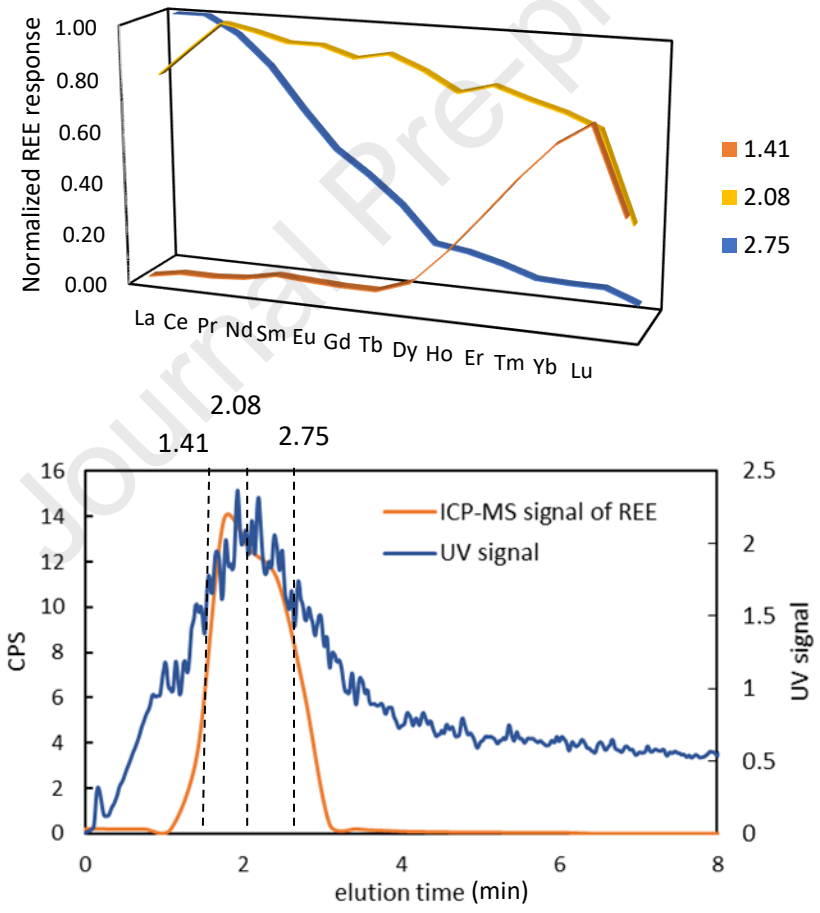

Figure 6. A) REE distribution in nano colloids based on the CPS and B) Overlaid fractograms of UV signal and CPS for nano colloids at different elution times at pH 6 and REE/Fe 0.1

Figure 6 exhibited the REE patterns (proportion of QQQ-ICP-MS CPS relative to the total REE QQQ-ICP-MS CPS at elution times) corresponding to the beginning (1.4 min), the maximum (2.1 min) and the end (2.7 min) of the UV signal. Beyond the steric effect, at 1.4 min, an enrichment in HREE with a maximum for Yb was observed, the QQQ-ICP-MS signal corresponded to 70 % of the total Yb CPS. At 2.1 min, the maximum of the UV signal, the QQQ-ICP-MS signal contained between 70 to 99% of the REE CPS. Finally, at 2.7 min, the end of the UV signal, the REE exhibited a strong decrease from La to Lu, with 99% of the total CPS corresponding to Ce and La. To sum up, at the beginning of the elution, nano-colloids were enriched in HREE, at the maximum of the UV signal, all REE were present with a small enrichment in MREE. At the end of the UV signal, nano-colloids were enriched in LREE and notably, La and Ce. Heavy REE have strongest affinity for organic colloids since able to form multidentate complexes as compared to LREE and MREE that form bidentate complexes (Marsac et al., 2010). These differential affinities result in a strong complexation of HREE and a weak complexation of LREE at the surface of the organic nano-colloids. At 1.4 min, since in steric elution mode, the main eluted HREE were then bound to the largest colloids. At 2.1 min, REE loading of nano-colloids with intermediary size were high and MREE were the most complexed REE (Marsac et al., 2010). Finally, since HREE were bound to the largest nano-colloids and because MREE have more affinity for OM binding sites than LREE, the smallest fraction of nano-colloids (eluted at 2.7 min) was enriched in LREE, exhibiting the lowest affinity for OM binding sites. This result could appear uncoherent as compared to the previous results of Tadayon et al. (2023) who explained that HREE have strong affinity for organic molecules <3kDa that compose the bulk Fe-OM colloids. But, these results are driven by the aggregation and the steric elution mode of the colloids. The REE patterns were here normalized by the total counts of the REE that passed through the channel, namely, without

considering the total concentration of REE and then the fraction <20kDa. At high REE/Fe ratio (0.1), colloids aggregated as a network in which REE made bridges between organic molecules and colloids. Since HREE display the highest affinity for OM binding sites amongst the whole REE group, and form strong complexes, they are the most efficient aggregating agents and allow the formation of the largest and strongest aggregates. By contrast, since LREE have the smallest affinity for OM, they form smallest and/or most fragile aggregates.

4 Implications, Limitations and Perspectives

This study demonstrated that REE form complexes with nano-colloids, implying a significant influence of these nano-colloids on the fate of REE. Being the most mobile fraction of colloids, nano-colloids can thus contribute to the transport of REE in the porosity of soils to water systems. However, while previous studies proposed that colloids govern the mobility and dissemination of REE (Dupré et al., 1999; Pédrot et al., 2008; O. Pokrovsky et al., 2006; Sholkovitz, 1995), the present results demonstrate that REE can modify colloid and nano-colloid structures by aggregation. Consequently, the fate of REE is determined, to some extent, by their own ability to aggregate colloids. Given the high affinity of HREE for binding to organic molecules and nano-colloids, especially at pH close to environmental pH (from 5 to 8), they appeared to be the most efficient REE in enhancing aggregation. However, HREE concentrations in the environment are lower than LREE (Mclennan, 1989), their impact on colloid aggregation could then be lower than expected from the present results. Further experiments with concentration distribution of REE similar to that observed and measured in the environment should then be performed.

411 The combined influence of REE and Ca on the colloids structure presents a complex landscape.
412 Major ions such as Ca involve colloid aggregation, potentially leading to larger aggregates. The
413 presence of REE reinforces this aggregation process, resulting in larger particle sizes.
414 Interestingly, like Ca, REE can act as aggregating agents. Both Ca and REE form bridges between
415 organic molecules. However, because Ca is a divalent alkaline earth while REEs are trivalent
416 metals, a higher concentration of Ca is required to achieve the same effect as REE. In the
417 environment, Ca is considered a major ion and is present in relatively high concentrations, whereas
418 REE are typically present as trace elements. Consequently, Ca is more likely to aggregate organic
419 matter (OM) and Fe-OM colloids due to its abundance. However, in contaminated environments
420 where the concentration of REE may be elevated, REE can become potentially significant
421 aggregating agents for colloids. This increased aggregation can subsequently limit the mobility of
422 the REE themselves, as they become part of larger, less mobile colloidal aggregates. The REE
423 loading appears thus to be a major parameter in the control of colloids and nano-colloids
424 aggregation. The OM concentration is also a parameter that can influence the colloid structure and
425 subsequent REE dynamics. In this study, the REE/OM ratio were ranged from 0.7 to 0.003 mol
426 mol^{-1}, aligning with ratios reported in diverse natural mediums with elevated OM concentrations.
427 Comparable ratios have been observed in shallow waters with REE/OM= 0.07-0.003 mol mol^{-1}
428 (Gruau et al., 2004; Pédrot et al., 2015; Pourret et al., 2010), in natural organic-rich waters with
429 REE/OM=0-0.01 mol mol^{-1} (Rey-Castro et al., 2009), and rivers with REE/OM=0.05-9×10^{-5} mol
430 mol^{-1} (Z. Xu & Han, 2009). This suggests that the REE/OM ratio explored in this study can be
431 found in various natural environments.

432 Therefore, investigations that span a diverse array of parameters including OM, REE and major
433 ions concentrations in the real environment have to be conducted. While this study focused on lab-

scale, it is essential to acknowledge that the behavior of colloids in the environment can be significantly more complex than in controlled conditions. For example, Slope et al. (Stolpe et al., 2013) from A4F-UV-ICPMS analysis of natural colloids demonstrated a variation in the chemical elements distribution in the nano-colloids fraction from spring flood to summer. Analyzing the nano-colloids size distributions with A4F-UV-ICP-MS from natural samples is thus needed to gain insights into how chemical elements and colloids interact in rivers and water. This study findings underscore the significant advantage of A4F-UV-QQQ-ICP-MS in delivering highly detailed and continuous colloidal size distributions of REE. The A4F-UV-ICPMS combination provides also more comprehensive insights into aquatic colloids compared to filtration and ultrafiltration techniques, which tend to segregate colloids into a limited number of fractions and which is subjected to clogging.

5 Conclusion

By exploring the complex interactions between pH, REE concentration, Ca, and nano-colloids using the A4F-UV technique, we gained insights into REE environmental dissemination. pH influenced nano-colloid structure: at pH 4, protonation led to colloid contraction or aggregation, while pH 6 showed a higher nano-colloid concentration. Calcium enhanced aggregation at both pH levels. The REE loading significantly contributed to aggregation, with REE acting as aggregating agents. While A4F did not provide detailed information on size fractionation under high REE concentrations due to steric mode elution, the coupling of A4F-UV with QQQ-ICP-MS revealed differential enrichment of HREE, MREE, and LREE within nano-colloids at pH 6.

Heavy REE, demonstrating a strong affinity and forming robust complexes with organic colloids, resulted in the formation of large nano-colloids. In contrast, LREE formed weaker bridges, leading to their association with smaller and weaker colloids. At low REE concentrations, inter-element competition diminished, allowing stochastic REE binding to nano-colloids without significant aggregation.

High REE concentrations lead to large aggregates, limiting mobility, whereas low concentrations allow stochastic binding without aggregation. The study underscores the importance of nano-colloids in REE mobility. Despite larger colloids being present, nano-colloids remain mobile and crucial for REE transport and distribution in environmental systems. Therefore, understanding nano-colloid behavior is essential for comprehensively understanding REE mobility in natural environments.

6 References

Afsar, M. Z., Yan, J., Vasilas, B., & Jin, Y. (2023). Redox oscillations destabilize and mobilize colloidal soil organic carbon. *Science of The Total Environment*, *864*, 161153. https://doi.org/10.1016/j.scitotenv.2022.161153

Au, K.-K., Penisson, A. C., Yang, S., & O'Melia, C. R. (1999). Natural organic matter at oxide/water interfaces: Complexation and conformation. *Geochimica et Cosmochimica Acta*, *63*(19–20), 2903–2917.

Baalousha, M. (2009). Aggregation and disaggregation of iron oxide nanoparticles: Influence of particle concentration, pH and natural organic matter. *Science of The Total Environment*, *407*(6), 2093–2101. https://doi.org/10.1016/j.scitotenv.2008.11.022

Baalousha, M., Manciulea, A., Cumberland, S., Kendall, K., & Lead, J. R. (2008). AGGREGATION AND SURFACE PROPERTIES OF IRON OXIDE NANOPARTICLES: INFLUENCE OF pH AND NATURAL ORGANIC MATTER. *Environmental Toxicology and Chemistry*, *27*(9), 1875. https://doi.org/10.1897/07-559.1

Bau, M. (1999). Scavenging of dissolved yttrium and rare earths by precipitating iron oxyhydroxide: Experimental evidence for Ce oxidation, Y-Ho fractionation, and lanthanide tetrad effect. *Geochimica et Cosmochimica Acta*, *63*(1), 67–77. https://doi.org/10.1016/S0016-7037(99)00014-9

Beauvois, A., Vantelon, D., Jestin, J., Bouhnik-Le Coz, M., Catrouillet, C., Briois, V., Bizien, T., & Davranche, M. (2021). How crucial is the impact of calcium on the reactivity of iron-organic matter aggregates? Insights from arsenic. *Journal of Hazardous Materials*, *404*, 124127. https://doi.org/10.1016/j.jhazmat.2020.124127

Beauvois, A., Vantelon, D., Jestin, J., Dupont, A., Briois, V., Paineau, E., Bizien, T., Pradel, A., & Davranche, M. (2023). Aluminum-induced colloidal destabilization of iron-organic matter nanoaggregates. *Geochimica et Cosmochimica Acta*, *344*, 1–11. https://doi.org/10.1016/j.gca.2023.01.005

Beauvois, A., Vantelon, D., Jestin, J., Rivard, C., Bouhnik-Le Coz, M., Dupont, A., Briois, V., Bizien, T., Sorrentino, A., Wu, B., Appavou, M.-S., Lotfi-Kalahroodi, E., Pierson-Wickmann, A.-C., & Davranche, M. (2020). How does calcium drive the structural organization of iron–organic matter aggregates? A multiscale investigation. *Environ. Sci.: Nano*, *7*(9), 2833–2849. https://doi.org/10.1039/D0EN00412J

Beckett, R., & Giddings, J. C. (1997). Entropic Contribution to the Retention of Nonspherical Particles in Field-Flow Fractionation. *Journal of Colloid and Interface Science*, *186*(1), 53–59. https://doi.org/10.1006/jcis.1996.4612

Buffle, J., & Leppard, G. G. (1995). Characterization of Aquatic Colloids and Macromolecules. 2. Key Role of Physical Structures on Analytical Results. *Environmental Science & Technology*, *29*(9), 2176–2184. https://doi.org/10.1021/es00009a005

Catrouillet, C., Guenet, H., Pierson-Wickmann, A.-C., Dia, A., LeCoz, M. B., Deville, S., Lenne, Q., Suko, Y., & Davranche, M. (2019). Rare earth elements as tracers of active colloidal organic matter composition. *Environmental Chemistry*, *17*(2), 133–139.

Chevalier, Q., El Hadri, H., Petitjean, P., Bouhnik-Le Coz, M., Reynaud, S., Grassl, B., & Gigault, J. (2018). Nano-litter from cigarette butts: Environmental implications and urgent consideration. *Chemosphere*, *194*, 125–130. https://doi.org/10.1016/j.chemosphere.2017.11.158

Christl, I. (2012). Ionic strength- and pH-dependence of calcium binding by terrestrial humic acids. *Environmental Chemistry*, *9*(1), 89. https://doi.org/10.1071/EN11112

Dahlqvist, R., Andersson, K., Ingri, J., Larsson, T., Stolpe, B., & Turner, D. (2007). Temporal variations of colloidal carrier phases and associated trace elements in a boreal river. *Geochimica et Cosmochimica Acta*, *71*(22), 5339–5354. https://doi.org/10.1016/j.gca.2007.09.016

Dai, S., Zhang, W., Dou, Y., Liu, H., Chen, X., Shi, J., & Dou, H. (2021). Towards a better understanding of the relationships between the structure and antitumor activity of Gastrodia elata polysaccharides by asymmetrical flow field-flow fractionation. *Food Research International*, *149*, 110673. https://doi.org/10.1016/j.foodres.2021.110673

Davranche, M., Pourret, O., Gruau, G., Dia, A., & Le Coz-Bouhnik, M. (2005). Adsorption of REE(III)-humate complexes onto MnO2: Experimental evidence for cerium anomaly and lanthanide tetrad effect suppression. *Geochimica et Cosmochimica Acta*, *69*(20), 4825–4835. https://doi.org/10.1016/j.gca.2005.06.005

Dia, A., Gruau, G., Olivié-Lauquet, G., Riou, C., Molénat, J., & Curmi, P. (2000). The distribution of rare earth elements in groundwaters: Assessing the role of source-rock composition, redox changes and colloidal particles. *Geochimica et Cosmochimica Acta*, *64*(24), 4131–4151. https://doi.org/10.1016/S0016-7037(00)00494-4

Dupré, B., Viers, J., Dandurand, J.-L., Polve, M., Bénézeth, P., Vervier, P., & Braun, J.-J. (1999). Major and trace elements associated with colloids in organic-rich river waters: Ultrafiltration of natural and spiked solutions. *Chemical Geology*, *160*(1–2), 63–80. https://doi.org/10.1016/S0009-2541(99)00060-1

Elderfield, H., Upstill-Goddard, R., & Sholkovitz, E. R. (1990). The rare earth elements in rivers, estuaries, and coastal seas and their significance to the composition of ocean waters. *Geochimica et Cosmochimica Acta*, *54*(4), 971–991. https://doi.org/10.1016/0016-7037(90)90432-K

Ferreira, M. D. S., Fontes, M. P. F., Bellato, C. R., Marques Neto, J. D. O., Lima, H. N., & Fendorf, S. (2021). Geochemical signatures and natural background values of rare earth elements in soils of Brazilian Amazon. *Environmental Pollution*, *277*, 116743. https://doi.org/10.1016/j.envpol.2021.116743

Forsyth, K., Dia, A., Marques, R., Prudêncio, M. I., Diamantino, C., Carvalho, E., Russo, D., Dionisio, I., Davranche, M., Bouhnik-Le-Coz, M., & Pédrot, M. (2023). Bioconcentration and translocation of rare earth elements in plants collected from three legacy mine sites in Portugal. *Frontiers in Environmental Science*, *11*, 1191909. https://doi.org/10.3389/fenvs.2023.1191909

Giddings, J. C. (1993). Field-Flow Fractionation: Analysis of Macromolecular, Colloidal, and Particulate Materials. *Science*, *260*(5113), 1456–1465. https://doi.org/10.1126/science.8502990

Gigault, J., El Hadri, H., Reynaud, S., Deniau, E., & Grassl, B. (2017). Asymmetrical flow field flow fractionation methods to characterize submicron particles: Application to carbon-based aggregates and nanoplastics. *Analytical and Bioanalytical Chemistry*, *409*(29), 6761–6769. https://doi.org/10.1007/s00216-017-0629-7

Gigault, J., Pettibone, J. M., Schmitt, C., & Hackley, V. A. (2014). Rational strategy for characterization of nanoscale particles by asymmetric-flow field flow fractionation: A tutorial. *Analytica Chimica Acta*, *809*, 9–24. https://doi.org/10.1016/j.aca.2013.11.021

Goyne, K. W., Brantley, S. L., & Chorover, J. (2010). Rare earth element release from phosphate minerals in the presence of organic acids. *Chemical Geology*, *278*(1–2), 1–14.

Gruau, G., Dia, A., Olivié-Lauquet, G., Davranche, M., & Pinay, G. (2004). Controls on the distribution of rare earth elements in shallow groundwaters. *Water Research*, *38*(16), 3576–3586. https://doi.org/10.1016/j.watres.2004.04.056

Guénet, H., Davranche, M., Vantelon, D., Pédrot, M., Al-Sid-Cheikh, M., Dia, A., & Jestin, J. (2016). Evidence of organic matter control on As oxidation by iron oxides in riparian wetlands. *Chemical Geology*, *439*, 161–172.

Halter, E., Montgomery, P., Montaner, D., Barillon, R., Del Nero, M., Galindo, C., & Georg, S. (2010). Characterization of inhomogeneous colloidal layers using adapted coherence probe microscopy. *Applied Surface Science*, *256*(21), 6144–6152. https://doi.org/10.1016/j.apsusc.2010.02.019

Hassellöv, M., & von der Kammer, F. (2008). Iron Oxides as Geochemical Nanovectors for Metal Transport in Soil-River Systems. *Elements*, *4*(6), 401–406. https://doi.org/10.2113/gselements.4.6.401

Kalinichev, A., & Kirkpatrick, R. (2007). Molecular dynamics simulation of cationic complexation with natural organic matter. *European Journal of Soil Science*, *58*(4), 909–917.

Kloster, N., Brigante, M., Zanini, G., & Avena, M. (2013). Aggregation kinetics of humic acids in the presence of calcium ions. *Colloids and Surfaces A: Physicochemical and Engineering Aspects*, *427*, 76–82.

Laveuf, C., & Cornu, S. (2009). A review on the potentiality of rare earth elements to trace pedogenetic processes. *Geoderma*, *154*(1–2), 1–12.

Lead, J. R., Davison, W., Hamilton-Taylor, J., & Buffle, J. (1997). Characterizing colloidal material in natural waters. *Aquatic Geochemistry*, *3*, 213–232.

Lead, J. R., Wilkinson, K. J., Lead, J. R., & Wilkinson, K. J. (2006). Aquatic Colloids and Nanoparticles: Current Knowledge and Future Trends. *Environmental Chemistry*, *3*(3), 159–171. https://doi.org/10.1071/EN06025

Li, F., Zhang, Q., Klumpp, E., Bol, R., Nischwitz, V., Ge, Z., & Liang, X. (2021). Organic Carbon Linkage with Soil Colloidal Phosphorus at Regional and Field Scales: Insights from Size Fractionation of Fine Particles. *Environmental Science & Technology*, *55*(9), 5815–5825. https://doi.org/10.1021/acs.est.0c07709

Li, X., Chen, Z., Chen, Z., & Zhang, Y. (2013). A human health risk assessment of rare earth elements in soil and vegetables from a mining area in Fujian Province, Southeast China. *Chemosphere*, *93*(6), 1240–1246.

Liu, H., Pourret, O., Guo, H., & Bonhoure, J. (2017). Rare earth elements sorption to iron oxyhydroxide: Model development and application to groundwater. *Applied Geochemistry*, *87*, 158–166. https://doi.org/10.1016/j.apgeochem.2017.10.020

Loell, M., Albrecht, C., & Felix-Henningsen, P. (2011). Rare earth elements and relation between their potential bioavailability and soil properties, Nidda catchment (Central Germany). *Plant and Soil*, *349*(1–2), 303–317. https://doi.org/10.1007/s11104-011-0875-y

Ma, L., Dang, D. H., Wang, W., Evans, R. D., & Wang, W.-X. (2019). Rare earth elements in the Pearl River Delta of China: Potential impacts of the REE industry on water, suspended particles and oysters. *Environmental Pollution*, *244*, 190–201. https://doi.org/10.1016/j.envpol.2018.10.015

Marsac, R., Davranche, M., Gruau, G., Bouhnik-Le Coz, M., & Dia, A. (2011). An improved description of the interactions between rare earth elements and humic acids by modeling: PHREEQC-Model VI coupling. *Geochimica et Cosmochimica Acta*, *75*(19), 5625–5637. https://doi.org/10.1016/j.gca.2011.07.009

Marsac, R., Davranche, M., Gruau, G., & Dia, A. (2010). Metal loading effect on rare earth element binding to humic acid: Experimental and modelling evidence. *Geochimica et Cosmochimica Acta*, *74*(6), 1749–1761. https://doi.org/10.1016/j.gca.2009.12.006

Marsac, R., Davranche, M., Gruau, G., Dia, A., Pédrot, M., Le Coz-Bouhnik, M., & Briant, N. (2013). Effects of Fe competition on REE binding to humic acid: Origin of REE pattern variability in organic waters. *Chemical Geology*, *342*, 119–127. https://doi.org/10.1016/j.chemgeo.2013.01.020

Mclennan, S. M. (1989). *Rare Earth Elements in Sedimentary Rocks: Influence of Provenance and Sedimentary Processes*.

Merschel, G., Bau, M., & Dantas, E. L. (2017). Contrasting impact of organic and inorganic nanoparticles and colloids on the behavior of particle-reactive elements in tropical estuaries: An experimental study. *Geochimica et Cosmochimica Acta*, *197*, 1–13. https://doi.org/10.1016/j.gca.2016.09.041

Müller, D., Cattaneo, S., Meier, F., Welz, R., & De Mello, A. J. (2015). Nanoparticle separation with a miniaturized asymmetrical flow field-flow fractionation cartridge. *Frontiers in Chemistry*, *3*. https://doi.org/10.3389/fchem.2015.00045

Nuttall, H. E., & Kale, R. (1993). Application of ESEM to environmental colloids. *Microscopy Research and Technique*, *25*(5–6), 439–446. https://doi.org/10.1002/jemt.1070250515

Ouatmane, A., Hafidi, M., Gharous, M. E., & Revel, J. (1999). Complexation of calcium ions by humic and fulvic acids. *Analusis*, *27*(5), 428–431.

Pédrot, M., Dia, A., & Davranche, M. (2010). Dynamic structure of humic substances: Rare earth elements as a fingerprint. *Journal of Colloid and Interface Science*, *345*(2), 206–213. https://doi.org/10.1016/j.jcis.2010.01.069

Pédrot, M., Dia, A., Davranche, M., Bouhnik-Le Coz, M., Henin, O., & Gruau, G. (2008). Insights into colloid-mediated trace element release at the soil/water interface. *Journal of Colloid and Interface Science*, *325*(1), 187–197.

Pédrot, M., Dia, A., Davranche, M., & Gruau, G. (2015). Upper soil horizons control the rare earth element patterns in shallow groundwater. *Geoderma*, *239*, 84–96.

Phelan, F. R., & Bauer, B. J. (2009). Comparison of steric effects in the modeling of spheres and rodlike particles in field-flow fractionation. *Chemical Engineering Science*, *64*(8), 1747–1758. https://doi.org/10.1016/j.ces.2008.10.006

Philippe, A., & Schaumann, G. E. (2014). Interactions of dissolved organic matter with natural and engineered inorganic colloids: A review. *Environmental Science & Technology*, *48*(16), 8946–8962.

Pokrovsky, O. S., & Schott, J. (2002). Iron colloids/organic matter associated transport of major and trace elements in small boreal rivers and their estuaries (NW Russia). *Chemical Geology*, *190*(1), 141–179. https://doi.org/10.1016/S0009-2541(02)00115-8

Pokrovsky, O. S., Viers, J., Shirokova, L. S., Shevchenko, V. P., Filipov, A. S., & Dupré, B. (2010). Dissolved, suspended, and colloidal fluxes of organic carbon, major and trace elements in the Severnaya Dvina River and its tributary. *Chemical Geology*, *273*(1–2), 136–149. https://doi.org/10.1016/j.chemgeo.2010.02.018

Pokrovsky, O., Schott, J., & Dupré, B. (2006). Trace element fractionation and transport in boreal rivers and soil porewaters of permafrost-dominated basaltic terrain in Central Siberia. *Geochimica et Cosmochimica Acta*, *70*(13), 3239–3260.

Pourret, O., Davranche, M., Gruau, G., & Dia, A. (2007a). Organic complexation of rare earth elements in natural waters: Evaluating model calculations from ultrafiltration data. *Geochimica et Cosmochimica Acta*, *71*(11), 2718–2735. https://doi.org/10.1016/j.gca.2007.04.001

Pourret, O., Davranche, M., Gruau, G., & Dia, A. (2007b). Rare earth elements complexation with humic acid. *Chemical Geology*, *243*(1–2), 128–141.

Pourret, O., Gruau, G., Dia, A., Davranche, M., & Molénat, J. (2010). Colloidal control on the distribution of rare earth elements in shallow groundwaters. *Aquatic Geochemistry*, *16*(1), 31–59.

Prestel, H., Schott, L., Niessner, R., & Panne, U. (2005). Characterization of sewage plant hydrocolloids using asymmetrical flow field-flow fractionation and ICP-mass spectrometry. *Water Research*, *39*(15), 3541–3552. https://doi.org/10.1016/j.watres.2005.06.027

Quinn, K. A., Byrne, R. H., & Schijf, J. (2006). Sorption of yttrium and rare earth elements by amorphous ferric hydroxide: Influence of solution complexation with carbonate. *Geochimica et Cosmochimica Acta*, *70*(16), 4151–4165. https://doi.org/10.1016/j.gca.2006.06.014

Rey-Castro, C., Mongin, S., Huidobro, C., David, C., Salvador, J., Garcés, J. L., Galceran, J., Mas, F., & Puy, J. (2009). Effective Affinity Distribution for the Binding of Metal Ions to a Generic Fulvic Acid in Natural Waters. *Environmental Science & Technology*, *43*(19), 7184–7191. https://doi.org/10.1021/es803006p

Roberts, G. C. (1975). The binding of substrates and inhibitors to dihydrofolate reductase. *Biochemical Society Transactions*, *3*(5), 630–631. https://doi.org/10.1042/bst0030630

Roberts, K. A., Santschi, P. H., Leppard, G. G., & West, M. M. (2004). Characterization of organic-rich colloids from surface and ground waters at the actinide-contaminated Rocky Flats Environmental

Technology Site (RFETS), Colorado, USA. *Colloids and Surfaces A: Physicochemical and Engineering Aspects*, *244*(1), 105–111. https://doi.org/10.1016/j.colsurfa.2004.06.009

Runyon, J. R., Ulmius, M., & Nilsson, L. (2014). A perspective on the characterization of colloids and macromolecules using asymmetrical flow field-flow fractionation. *Colloids and Surfaces A: Physicochemical and Engineering Aspects*, *442*, 25–33. https://doi.org/10.1016/j.colsurfa.2013.04.010

Ryan, J. N., & Elimelech, M. (1996). Colloid mobilization and transport in groundwater. *Colloids and Surfaces A: Physicochemical and Engineering Aspects*, *107*, 1–56. https://doi.org/10.1016/0927-7757(95)03384-X

Saito, T., Suzuki, Y., & Mizuno, T. (2013). Size and elemental analyses of nano colloids in deep granitic groundwater: Implications for transport of trace elements. *Colloids and Surfaces A: Physicochemical and Engineering Aspects*, *435*, 48–55. https://doi.org/10.1016/j.colsurfa.2012.11.031

Schijf, J., & Marshall, K. S. (2011). YREE sorption on hydrous ferric oxide in 0.5M NaCl solutions: A model extension. *Marine Chemistry*, *123*(1–4), 32–43. https://doi.org/10.1016/j.marchem.2010.09.003

Schimpf, M. E., Caldwell, K., & Giddings, J. C. (2000). *Field-Flow Fractionation Handbook*. Wiley. https://books.google.fr/books?id=zJzJvs4LQAwC

Sholkovitz, E. R. (1995). The aquatic chemistry of rare earth elements in rivers and estuaries. *Aquatic Geochemistry*, *1*(1), 1–34. https://doi.org/10.1007/BF01025229

Skliar, M., & Chernyshev, V. S. (2019). Imaging of Extracellular Vesicles by Atomic Force Microscopy. *JoVE (Journal of Visualized Experiments)*, *151*, e59254. https://doi.org/10.3791/59254

675 Sonke, J. E. (2006). Lanthanide−Humic Substances Complexation. II. Calibration of Humic Ion-
676 Binding Model V. *Environmental Science & Technology*, *40*(24), 7481–7487.
677 https://doi.org/10.1021/es060490g

678 Stolpe, B., Guo, L., & Shiller, A. M. (2013). Binding and transport of rare earth elements by organic
679 and iron-rich nanocolloids in Alaskan rivers, as revealed by field-flow fractionation and ICP-MS.
680 *Geochimica et Cosmochimica Acta*, *106*, 446–462. https://doi.org/10.1016/j.gca.2012.12.033

681 Strakhovenko, V., Belkina, N., Subetto, D., Rybalko, A., Efremenko, N., Kulik, N., Potakhin, M.,
682 Zobkov, M., Ovdina, E., & Ludikova, A. (2023). Distribution of rare earth elements and yttrium in water,
683 suspended matter and bottom sediments in Lake Onego: Evidence of the watershed transformation in the
684 Late Pleistocene. *Quaternary International*, *644–645*, 120–133.
685 https://doi.org/10.1016/j.quaint.2021.07.011

686 Tadayon, Y., Vantelon, D., Gigault, J., Dia, A., Pattier, M., Dutruch, L., & Davranche, M. (2024). Rare
687 earth elements interaction with iron-organic matter colloids as a control of the REE environmental
688 dissemination. *Journal of Colloid and Interface Science*, *655*, 70–79.
689 https://doi.org/10.1016/j.jcis.2023.10.110

690 Tang, S., Zheng, C., Chen, M., Du, W., & Xu, X. (2020). Geobiochemistry characteristics of rare earth
691 elements in soil and ground water: A case study in Baotou, China. *Scientific Reports*, *10*(1), 11740.
692 https://doi.org/10.1038/s41598-020-68661-4

693 Town, R. M., Duval, J. F. L., Buffle, J., & van Leeuwen, H. P. (2012). Chemodynamics of Metal
694 Complexation by Natural Soft Colloids: Cu(II) Binding by Humic Acid. *The Journal of Physical Chemistry*
695 *A*, *116*(25), 6489–6496. https://doi.org/10.1021/jp212226j

Vasyukova, E. V., Pokrovsky, O. S., Viers, J., Oliva, P., Dupré, B., Martin, F., & Candaudap, F. (2010). Trace elements in organic- and iron-rich surficial fluids of the boreal zone: Assessing colloidal forms via dialysis and ultrafiltration. *Geochimica et Cosmochimica Acta*, *74*(2), 449–468. https://doi.org/10.1016/j.gca.2009.10.026

Wagner, M., Holzschuh, S., Traeger, A., Fahr, A., & Schubert, Ulrich. S. (2014). Asymmetric Flow Field-Flow Fractionation in the Field of Nanomedicine. *Analytical Chemistry*, *86*(11), 5201–5210. https://doi.org/10.1021/ac501664t

Walther, C. (2003). Comparison of colloid investigations by single particle analytical techniques—A case study on thorium-oxyhydroxides. *Colloids and Surfaces A: Physicochemical and Engineering Aspects*, *217*(1–3), 81–92. https://doi.org/10.1016/S0927-7757(02)00562-9

Xu, H., Lin, H., Jiang, H., & Guo, L. (2018). Dynamic molecular size transformation of aquatic colloidal organic matter as a function of pH and cations. *Water Research*, *144*, 543–552.

Xu, Z., & Han, G. (2009). Rare earth elements (REE) of dissolved and suspended loads in the Xijiang River, South China. *Applied Geochemistry*, *24*(9), 1803–1816. https://doi.org/10.1016/j.apgeochem.2009.06.001

Yang, Z., Gao, B., & Yue, Q. (2010). Coagulation performance and residual aluminum speciation of Al2(SO4)3 and polyaluminum chloride (PAC) in Yellow River water treatment. *Chemical Engineering Journal*, *165*(1), 122–132. https://doi.org/10.1016/j.cej.2010.08.076

Highlights:

- A4F-UV-QQQ-ICP-MS shows REE fractionation within nano-colloids.
- Heavy REE act as effective aggregating agents for nano-colloids.
- Light REE form weak bridges, binding to the smallest, least robust nano-colloids.
- REE loading significantly enlarges the aggregation of nano-colloids.
- REE ability to induce colloidal aggregation controls their environmental mobility.

Declaration of interests

☒ The authors declare that they have no known competing financial interests or personal relationships that could have appeared to influence the work reported in this paper.

☐ The authors declare the following financial interests/personal relationships which may be considered as potential competing interests: